Spiliopoulos, Panagiotis; Navarro, Saül Llàcer; Orzan, Eliott; Ghanbari, Reza; Pietschnig, Rudolf; Stilianu, Clemens; Spirk, Stefan; Schaefer, Andreas; Kádár, Roland; Nypelö, Tiina

Cellulose modified to host functionalities via facile cation exchange approach

Published in:
Carbohydrate Polymers

DOI:
10.1016/j.carbpol.2024.121857

Published: 15/05/2024

Document Version
Publisher's PDF, also known as Version of record

Carbohydrate Polymers 332 (2024) 121857

Contents lists available at ScienceDirect

Carbohydrate Polymers

journal homepage: www.elsevier.com/locate/carbpol

Cellulose modified to host functionalities via facile cation exchange approach

Panagiotis Spiliopoulos [a,b], Saül Llàcer Navarro [a,b], Eliott Orzan [a], Reza Ghanbari [c], Rudolf Pietschnig [d], Clemens Stilianu [e], Stefan Spirk [f], Andreas Schaefer [a], Roland Kádár [c,b], Tiina Nypelö [a,b,g,*]

[a] Department of Chemistry and Chemical Engineering, Chalmers University of Technology, Gothenburg, Sweden
[b] Wallenberg Wood Science Center (WWSC), Chalmers University of Technology, Gothenburg, Sweden
[c] Department of Industrial and Materials Science, Chalmers University of Technology, Gothenburg, Sweden
[d] Institute of Chemistry and CINSaT, University of Kassel, Kassel, Germany
[e] Institute of Biomedical Imaging, Graz University of Technology, Graz, Austria
[f] Institute of Bioproducts and Paper Technology, Graz University of Technology, Graz, Austria
[g] Department of Bioproducts and Biosystems, Aalto University, Espoo, Finland

ARTICLE INFO

Keywords:
Lanthanides
Rheology
Luminescence

ABSTRACT

Properties of cellulose are typically functionalized by organic chemistry means. We progress an alternative facile way to functionalize cellulose by functional group counter-cation exchange. While ion-exchange is established for cellulose, it is far from exploited and understood beyond the most common cation, sodium. We build on our work that established the cation exchange for go-to alkali metal cations. We expand and further demonstrate the introduction of functional cations, namely, lanthanides. We show that cellulose nanocrystals (CNCs) carrying sulfate-half ester groups can acquire properties through the counter-cation exchange. Trivalent lanthanide cations europium (Eu^{3+}), dysprosium (Dy^{3+}) and gadolinium (Gd^{3+}) were employed. The respective ions showed distinct differences in their ability of being coordinated by the sulfate groups; with Eu^{3+} fully saturating the sulfate groups while for Gd^{3+} and Dy^{3+}, values of 82 and 41 % were determined by compositional analysis. CNCs functionalized with Eu^{3+} displayed red emission, those containing Dy^{3+} exhibited no optical functionality, while those with Gd^{3+} revealed significantly altered magnetic relaxation times. Using cation exchange to alter cellulose properties in various ways is a tremendous opportunity for modification of the abundant cellulose raw materials for a renewable future.

1. Introduction

Cellulose consists of anhydroglucose units linked at high degree of polymerization via β-1,4-glycosidic bonds. The versatile properties of cellulose can be chemically manipulated by modifying the hydroxyl groups at C2, C3 and C6, the glycosidic bond, opening the glucose ring and by modifying the reducing end group. (Klemm, Philipp, Heinze, Heinze, & Wagenknecht, 1998) Cellulose often undergoes chemical modification during its processing when it is liberated from plant biomass through chemical and thermal means.(Sixta, 2006) Sulfur compounds are used in many of these processes and they may result in sulfonation and sulfation of the wood components. Sulfate groups are present in nanocelluloses due to manufacturing using sulfuric acid. (Habibi, Lucia, & Rojas, 2010) Many cellulose products such as the pulp fibers contain carboxyl groups as a result of oxidation or having residual amounts of other plant polysaccharides. Hence, charged functional groups are commonly found in cellulose materials.

We employ exchanging a counter-cation of sulfate half-ester groups on cellulose to functionalize cellulose. The approach is straightforward, but it holds the requirement of selecting a cellulosic material that contains functional groups that have an ion or a proton to exchange.(Petschacher et al., 2022) The material – acting as a host, is exposed in a dispersion to an excess of the selected cation and the exchange is facilitated by increase of pH (neutralization). The product is subsequently purified by dialysis. The selected substrate for demonstrating the modification is cellulose nanocrystals (CNCs) which are anisotropic

* Corresponding author at: Department of Chemistry and Chemical Engineering, Chalmers University of Technology, Kemivägen, 41296 Gothenburg, Sweden.
E-mail address: tiina.nypelo@aalto.fi (T. Nypelö).

https://doi.org/10.1016/j.carbpol.2024.121857
Received 7 November 2023; Received in revised form 12 January 2024; Accepted 21 January 2024
Available online 22 January 2024

colloidal nanoparticles. We have demonstrated the cation exchange for sulfated CNCs for the alkali metal cations (Petschacher et al., 2022). Prior to our endeavors, the proton or cation exchange was established, for example for sulfate groups for the proton exchange to Na, K, and Cs (Dong & Gray, 1997) and for analytical purposes to determine functional group content (Abitbol, Kloser, & Gray, 2013; Beck, Méthot, & Bouchard, 2015; Dong, Revol, & Gray, 1998). Our approach enabled to omit employment of ion exchange resins and hence simplified the modification method and demonstrated the introduction of the first group cations (excluding radioactive Francium).

The unique electronic structure of lanthanides endows them with remarkable properties, including luminescence and magnetism.(Cotton, 2013; Werts, 2005) A material can become luminescent via successful association with lanthanides. Europium has been used as a luminescent probe in bioimaging and gadolinium in magnetic resonance imaging. (Teo, Termini, & Gray, 2016) Lanthanides embedded in cellulose materials have led to the successful identification of fibers via luminescence.(Skwierczyńska, Runowski, Kulpiński, & Lis, 2019; Szczeszak et al., 2020; Wang et al., 2018) The challenge lies in finding a way to introduce the ions while keeping the luminescence and the material intact. Regenerated cellulose fibers loaded with 2 % by weight of Eu^{3+} exhibiting the characteristic emission band at 592 nm, were used for demonstrating the successful combination of both features.(Skwierczyńska et al., 2019) Hence, fabrics made using these fibers could be tagged with a unique luminescent probe. Yb^{3+} and Er^{3+} nanoparticles embedded in regenerated cellulose fibers emit bright green light when exposed to near-infrared wavelengths (975 nm).(Szczeszak et al., 2020) Cellulose pulp fibers doped with Eu^{3+} via polymer retention were employed for anticounterfeiting (Wang et al., 2018).

The incorporation of lanthanide ions into cellulose has relied on carboxyl groups. Incubation of carboxymethylated cellulose derivate and its hydrogel in lanthanide chloride solutions allowed for binding between lanthanide ions and the carboxyl groups on the cellulose framework.(Fan, Du, Kou, Zhang, & Liu, 2018) Carboxylated nanofibrillated cellulose films have been functionalized with Yb^{3+} and Nd^{3+} complexes to generate a UV filter with luminescence in the near-infrared range.(Xue et al., 2018) Similarly, carboxyl groups coordinated with Eu, Sm, and Tb produce a luminescence effect.(Miao et al., 2015; Yang et al., 2018; Zhang, Liu, Chang, Li, & Zhang, 2019).

We employ the cation exchange method to coordinate Eu^{3+}, Gd^{3+}, and Dy^{3+} with the sulfate groups on the CNC surface hypothesizing that this can be done in a similar manner as achieved with carboxyl groups. The aim of our work is to extend the cation-exchange as a concept for cellulose modification, that in the future can be utilized for a broad range of functional groups and various cations.

The lanthanides were used as salts to ensure modification in water. Lanthanides are commonly used in catalysis and in, e.g., magnets and hence available, although sustainable mining or supply via recycling routes needs to be considered. Gadolinium salts are routinely used in magnetic resonance imaging (MRI) as contrast agents costing currently from 60 up to 1700 USD/kg (according to e.g. chemimpax.com). It has a rather high LD_{50} value, >2 g/kg (pubchem.org) indicating non-toxicity. According to (Rim, Koo, & Park, 2013) free ions of gadolinium are toxic, and hence in MRI are always chelated. Europium salts are used in cathode ray tube coatings and in nuclear magnetic resonance (NMR) spectroscopy. The price is up to 760 USD/kg (chemicalbook.com). $EuCl_3$ is toxic to aquatic life and has oral LD_{50} value of 3527 mg/kg.(pubchem.org) According to (Rim et al., 2013) There are no clear indications that europium is particularly toxic compared to other heavy metals. Dysprosium is used in laser materials and as an intermediate to other dysprosium compounds. Dysprosium chloride costs up to 1700 USD/kg (chemicalbook.com). Dysprosium chloride is mildly toxic when ingested. The oral LD_{50} value is 5443 mg/kg.(pubchem.org).

Eu^{3+} and Dy^{3+} were selected because of their characteristic red and yellow luminescence when coordinated with ligands; whereas Gd^{3+} was outlined due to its magnetic properties. The approach is readily applicable to sulfate groups providing an intriguing concept for a straightforward one-step modification pathway.

2. Experimental

2.1. Materials

Cellulose nanocrystals (CNCs) were purchased from Celluforce (Canada). CNCs consist of cellulose and they are rod-like particles with diameter of approximately 4 nm and lengths between 100 and 200 nm. The CNCs (Na-CNCs) carry sulfate half-ester groups with degree of surface substitution of 15 % that were neutralized with sodium as a result of the manufacturing process.(Llàcer Navarro et al., 2021) According to elemental composition, there is approximately 0.6 wt% sulfur in the CNCs (Supporting information Table S1). The total acid group content was at least 0.20 mmol/g according to conductometric titration. (Llàcer Navarro, Tõlgo, Olsson, & Nypelö, 2023) To obtain protonated CNCs (H-CNC), HCl was added until the suspension reached pH 2 and the suspension was then purified by dialysis. Europium (III) chloride hexahydrate (99.99 %), gadolinium (III) chloride hexahydrate (99 %), and dysprosium (III) chloride hexahydrate (99.9 %) were purchased from Sigma Aldrich (Sweden).

2.2. Cellulose nanocrystal lanthanide modification

Lanthanide (Ln) chloride solutions (1 wt%) were prepared in ultrapure water. These solutions were subsequently introduced into Na-CNC suspensions at 2.25 wt% CNC. These concentrations were chosen so that their viscosity would not prohibit stirring and dialysis but at the same time to be sufficiently high to allow scaling up. The lanthanides were added in excess with the aim of complete exchange to achieve a sulfur (S)/Ln atomic ratio of 3:1. The suspensions were stirred overnight followed by dialysis through SpectraPor membranes (VWR, Sweden) with a cut-off of 12,000–14,000 g/mol.

2.3. Characterization

2.3.1. Determination of lanthanide loading

Elemental analysis was carried out in duplicate by Mikrolab Kolbe (Oberhausen, Germany). X-ray photoelectron spectroscopy (XPS) was performed using a PHI 5000 VersaProbe III Scanning XPS Microprobe. Dried powders of the suspensions were mounted on a stainless steel sample holder and fixed with a perforated stainless steel mask. Charging effects were compensated by simultaneous use of an electron flood gun and Ar^+ ion gun. All binding energy values reported are referenced to the leading peak in the deconvoluted C 1*s* spectra and are set at 286.7 eV for C-O in cellulose.(Johansson, Campbell, & Rojas, 2020) C 1*s* spectra were deconvoluted using Voigt profiles after subtracting a Shirley type background. The width of the Lorentzian contribution was fixed. (Campbell & Papp, 2001) The surface concentration of elements was obtained with MultiPak software (version 9.6.0.15; PHI) using atomic sensitivity factors.

Energy-dispersive X-ray spectroscopy (EDX) was used to assess the elemental composition of the films. A JEOL 7800F Prime scanning electron microscope with an EDX attachment was used to scan the film surface at an acceleration voltage of 20 kV in order to accurately monitor lanthanide content. Oxford AZtec was used to calculate the atomic % using 15 sample points from three individual scans of each Ln-CNC film.

For visual inspection, 250 microliters Ln-CNC suspensions were placed on soda lime glass discs (Thermo Scientific, Menzel-Gläser) and examined under a Zeiss Imager Z2m polarized optical microscope with a 100× magnifying lens and at 5200 ms exposure time.

2.3.2. Rheology

An Anton Paar (Austria) MCR 702 Twin Drive rheometer was used

for rheological measurements. Steady shear tests were performed in a single motor-transducer configuration equipped with a P-PTD200/ glass measuring cell. All measurements were performed at room temperature, 23 °C, via a Peltier device included in the bottom plate assembly. A parallel-plate glass measuring geometry with a diameter of 43 mm at a measuring gap of 1 mm was used within a shear rate range of 10^{-3} to 10^{3} s^{-1}. Oscillatory shear tests were conducted using the same configuration with a 50 mm diameter plate geometry and a measuring gap of 1 mm. The strain amplitude sweep tests were conducted within a strain amplitude range of 10^{-3} % to 10^{3} % at a constant angular frequency of 6.28 rad/s. Linear viscoelastic frequency sweep tests were performed in a separate-motor transducer configuration using two parallel-plate 50 mm measuring geometry operated in counter-oscillation mode. The angular frequency range was 10^{-3} to $8{\cdot}10^{2}$ rad/s at a constant strain amplitude of 0.25 % based on strain sweep tests.

2.3.3. Zeta potential determination

The Zeta potential of the dispersions was determined using the Zetasizer Nano (Malvern, UK). The measurements were performed at 25.0 ± 0.1 °C in 0.1 M sodium acetate buffer at pH 4, with 0.25 wt% CNC suspensions. Up to 5 mM NaCl was added to ensure that the thickness of the double layer surrounding the CNC was not infinite. Data were processed by Malvern Zetasizer Software v7.13. The zeta potential was calculated as the average of six measurements, each of them comprising 30 to 150 sub-runs.

2.3.4. Optical, magnetic and thermal properties

For thermal gravimetric analysis (TGA), CNC suspensions were dried and characterized using a Mettler Toledo - TGA/DSC instrument. Nitrogen or air flow was set to 100 mL/min and the heating rate to 10 K/min. Assay temperatures ranged from room temperature to 600 °C.

UV–visible absorption and transmission measurements were carried out using a Cary 60 UV–Vis spectrometer (G6860A; Agilent Technologies), with average time of 0.1 s, data interval of 1 nm, and scan rate of 600 nm/min at dual beam mode. Scan software was used for data acquisition. The suspensions were loaded into UV–Vis quartz crystal cuvettes (10 × 10 mm) from Hellma Analytics. A UVP Transilluminator PLUS (Analytik Jena) was employed for luminescence measurements An FL3–22 fluorophotometer and Fluorog spectrophotometer equipped with a 450 W FL-1039 A/40 A illuminator (Horiba Scientific) and a CARON (2050 W) detector cooling unit were used for fluorescence measurements. FluorEssence V3.8 software was used for data acquisition. All measurements took place at room temperature.

Magnetic relaxation times of Gd-CNC suspensions were estimated using a 7 T Bruker BioSpec 70/30 preclinical scanner, based on a built-in Bruker sequence fitted through five points.

3. Results and discussion

3.1. Degree of modification of CNCs with lanthanides

The cellulose substrate contained 0.63 wt% sulfur (Supporting information Table S1). Considering that the sulfate half-ester groups can be located only on the CNC surface, approximately 15 % of the surface anhydroglucose units is estimated to carry a sulfate half-ester group. (Llàcer Navarro et al., 2021; Llàcer Navarro et al., 2023) The cellulose substrates were targeted for the highest degree of modification achievable, which was assumed to be three times the degree of sulfation. Lower inclusion levels may be possible to be introduced either by lowering the cation concentration, reaction time or the sulfate half-ester group content of the substrate.

An excess of cations was used and a combination of elemental analysis, XPS, and EDX was used to quantify the incorporation of Eu^{3+}, Dy^{3+} and Gd^{3+} in CNC suspensions (Fig. 1 and Supporting information Tables S1–S3).

Both elemental analysis and XPS revealed a similar trend regarding the inclusion levels with Dy^{3+} exhibiting the lowest incorporation level (Fig. 1). Instead, EDX analysis revealed no significant difference in inclusion levels of the three lanthanides. Sulfates, and hence, lanthanide ions are assumed to be located exclusively on the surface where esterification occurs, since these nanoparticles are, in fact, impermeable. This may explain why the inclusion level of sulfate and lanthanide ions measured by XPS was two and ten times higher, respectively, than what was obtained by elemental analysis. However, the values >1 observed using XPS, as representative for the surface composition, do indicate that metal cations might also be connected to different sites apart from the sulfate groups or that other chemical species form.

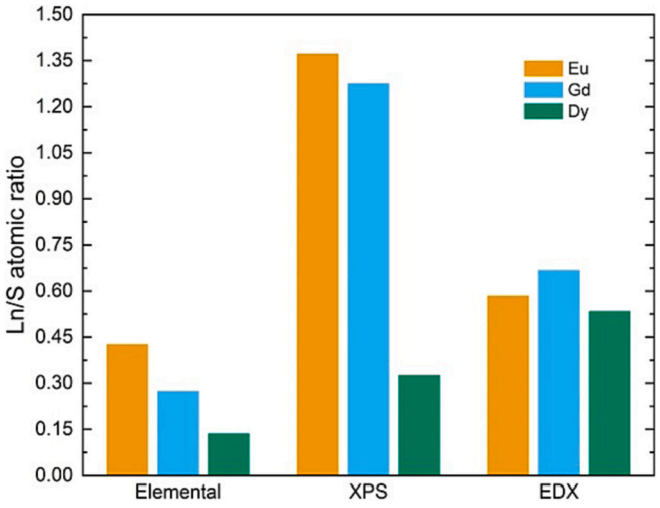

Fig. 1. Ln to S (atomic/molar) ratio in CNCs based on elemental analysis, EDX, and XPS.

3.2. Regarding the Ln^{3+} interaction with CNCs

Films made from CNC alone did not exhibit a specific absorbance within 200–800 nm range. In contrast, inclusion of Ln cations modified the coordination environment and caused absorption at 285 nm (Fig. 2). Nanocellulose decorated with carboxyl groups and loaded with lanthanides has been reported firstly to show absorbance caused by the carbonyls and secondly both to shift and not to shift that absorbance following the inclusion of lanthanides.(Ye, Wang, Xiong, & Sun, 2016;

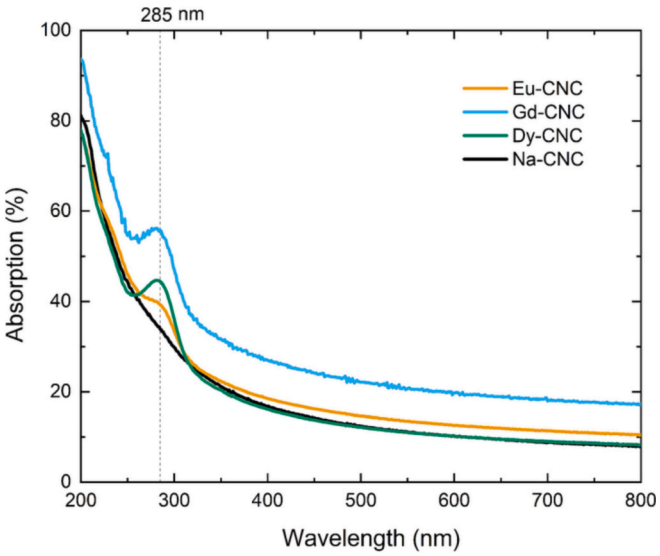

Fig. 2. UV–Vis absorption spectra of Na-CNC and Ln-CNC films.

Zhang et al., 2019) The inclusion of the three different lanthanides led to absorption at the same wavelength. One may think to consider the possibility that the Lewis acid trivalent ions lead to elimination of HSO_4^-. However, according to the elemental analysis the sulfur content did not decrease with the modification (Supporting information Table S1) and hence, it does not indicate that the cellulose sulfate half-ester group content was modified.

The thermal stability of CNC films was evaluated by TGA, which revealed the onset of thermal degradation (T_{onset}) for the different CNC films (Fig. 3). For the H-CNC films, T_{onset} was 200 °C; whereas for Na-CNC films, it was 255 °C, indicating improved tolerance towards thermal decomposition when the sodium was present. Sulfate half-ester groups act as dehydration catalysts for CNCs, promoting the decomposition of H-CNC films. The sodium present on Na-CNCs prevents the dehydration process and, as a result, a higher T_{onset} is observed.(Roman & Winter, 2004; Vanderfleet et al., 2019; Wang, Ding, & Cheng, 2007) The introduction of lanthanides lowered T_{onset} to 160 °C, suggesting an enhanced dehydration process, due to combination with the sulfate half-ester groups in the CNCs, leading to degradation in lower temperatures.

The effect of lanthanides on thermal stability is not always negative. Eu-coordination with the COO^- group has been reported to improve the thermal resistance of cellulose, from 245 to 305 °C.(Yang et al., 2018) In contrast, no significant difference in thermal stability was observed between carboxylated nanocellulose materials containing or not Eu^{3+} with degradation starting at around 220 °C in either case.(Miao et al., 2015) In a study of carboxymethyl cellulose-Ln complexes, the material remained thermally stable until 250 °C;(Fan et al., 2018) however, no comparison to cellulose was conducted. Finally, in non-carboxylated nanocellulose, the introduction of another lanthanide such as Yb did not alter thermal degradation, which began irrespectively at 300 °C.

Detailed photoelectron spectra were recorded for C 1*s*, S 2*p*, O 1*s*, and Ln 4*d* levels. As shown in Fig. 4, the C 1*s* signals were fitted with four components centered at 285.2, 286.7, 288.1, and 289.3 eV, which corresponded to carbon in C-C, C-O, O-C-O, and O-C=O bonding configurations, respectively.(Johansson et al., 2020) The spectra reflect a typical signature for cellulose with additional C-C, most likely from environmental contamination during sample storage and transfer. Similar features and contamination levels were observed in the C 1*s* spectrum of ashless Whatman 42 cellulose filter paper (Supporting information Fig. S1). Hence, addition of Ln^{3+} has no detectable effect on the pattern of C 1*s* spectra. The S 2*p* spectra shown in Fig. 4 are positioned at a binding energy typical for sulfur in SO_4^{2-} (Moulder, Stickle, Sobol, & Bomben, 1992). In the case of Gd-CNCs, a final state satellite signal from the Gd 4*d* level overlaps with the S 2*p* signal. Both, C 1*s* and S 2*p* spectra indicate no variation between different Ln loadings. The same trend was observed for the O 1*s* spectra (Supporting information Fig. S2), confirming the lack of significant differences between the three samples and the reference filter paper. A detailed evaluation of Ln 4*d* (Supporting information Fig. S3) was difficult as all lanthanide spectra exhibit a complex final state satellite structure. Those spectral features can be indicative for the presence of various oxidized species and an unambiguous assignment based on our data is difficult. The spectrum of Eu 4*d* stood out owing to a strong shake-down satellite signal previously described only for Eu-oxalate systems. For $Eu_2(SO_4)_3$, this satellite signal is normally of minor intensity.(Mercier, Alliot, Bion, Thromat, & Toulhoat, 2006) We exclude the presence of Eu^{2+} being responsible for that signal as Eu^{2+} can be obtained only using harsh reduction agents such as elemental metals (e.g. Zn, Li) or hydrides (LiH) which were not employed in our case.(Brauer, 1960) Hence, the coordination of Eu^{3+} by CNC-SO_4 groups appears different from that of pure Eu(III) sulfate. The literature on the shake-down satellite in europium compounds is limited and there is no plausible explanation for its appearance in systems like $Eu_2(C_2O_4)_3$ so far in the scientific community. XRD data for the corresponding lanthanide sulfates has shown that the lanthanides are coordinated in an 8-fold manner (Eu^{3+}, Gd^{3+}, Dy^{3+}), (Denisenko et al., 2022; Hummel, Fischer, Fischer, Joerg, & Pezzei, 1993) with water being used to saturate the Ln-coordination sphere. The XPS spectra confirm that there are several lanthanide species present in the Ln-CNCs. The presence of oxidic species, particularly for Eu-CNC complicates a quantitative analysis. Apart from Eu^{2+}, which has been excluded based on the used chemistry, another option is that not all of the $EuCl_3$ has been dialyzed out. However, we did not observe significant amounts of europium chloride in the XPS spectra. It seems plausible that there is some oxidic europium compounds (e.g., europium hydroxides, mixed oxides, Eu_2O_3) deposited on the surface. Apart from XPS, elemental analysis can also be employed to estimate the coordination numbers of the lanthanides to the sulfates. The lanthanides have a charge of +3, consequently they must interact with three sulfate groups, either on the

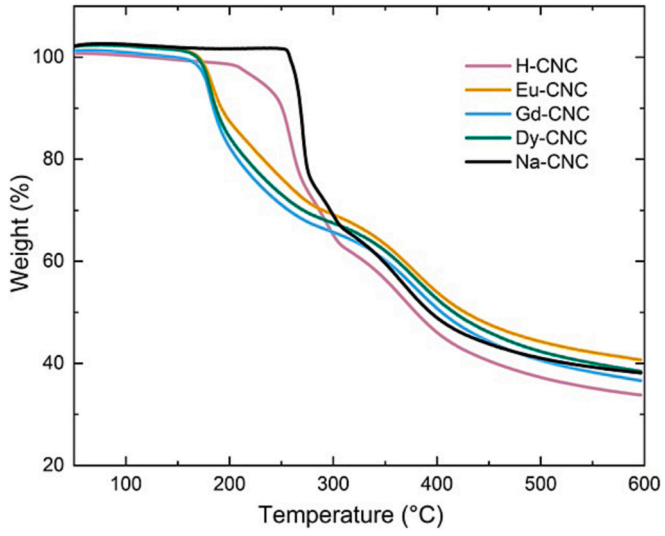

Fig. 3. TGA of H-CNC, Na-CNC, and Ln-CNC films.

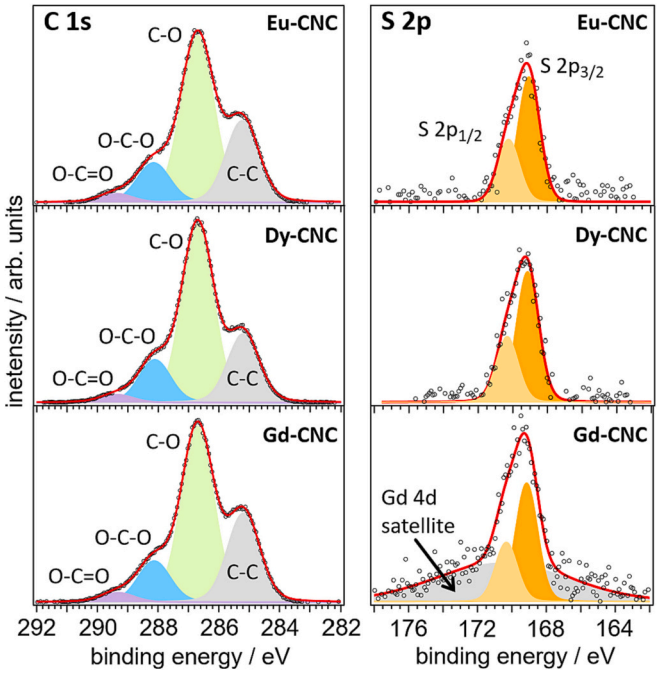

Fig. 4. C 1*s* and S 2*p* core level spectra. The measured data is represented by open circles and the fit result as the solid red line. The individual spectral components originating from carbon atoms in C-C, C-O, O-CO, and O-C=O bonding configurations are shown as shaded curves. (For interpretation of the references to colour in this figure legend, the reader is referred to the web version of this article.)

same CNC or on different ones to neutralize the overall charge on the CNCs. Additional coordination sites typically stem from water molecules or hydroxyls, providing hard oxygen donors to the hard lanthanide ions. By calculation of the molar ratio of the S/Ln, the coordination of the different lanthanides can be estimated. When the factor of three is considered (as one Ln^{3+} is coordinated by three sulfate groups), the extent of effective cation exchange can be determined. Dy^{3+} coordinates to 41 % of the available sulfate groups, while in Gd-CNC 82 % of the sulfate groups are charge neutralized by Gd^{3+}. In the Eu-CNC, 127 % of the sulfates are saturated by the Eu^{3+}. Hence, the Ln^{3+} cations are exchanged to different extents relative to the sulfate groups. The XPS spectra demonstrate that the Ln^{3+} ions attached to the sulfated CNCs have a different coordination environment compared to the pure $Ln_2(SO_4)_3$ species.

3.3. Properties of CNC suspensions

At critical concentration (here 4 wt%), CNCs self-assemble into liquid crystal phases that can be identified via polarized optical microscopy.(Kádár, Fazilati, & Nypelö, 2020) As expected, the unmodified Na-CNC suspension at <2 % concentration did not display any polarization patterns (Supporting information Fig. S4a). However, the introduction of lanthanide cations altered the system, demonstrating a drastic change in the polarization pattern (Supporting information Fig. S4b–d).

The observed transition in polarization at such low inclusion levels may be ascribed to changes in colloidal stability due to the electrical environment of sulfate groups. Na^+ or Ca^{2+} have been shown efficiently to suppress the electric double layer between CNCs and lower the suspension's zeta potential, even reversing it from negative to positive. (Prathapan, Thapa, Garnier, & Tabor, 2016; Zhong, Fu, Peng, Zhan, & Sun, 2012) The H-CNC suspension exhibited a zeta potential of −27 mV (Fig. 5). Addition of Ln^{3+} ions increased the zeta potential to approximately −22 mV, with almost negligible variations between the Ln cations, which is expected since there should not be significant differences between them in this respect. The increase in zeta potential can be explained by Ln^{3+} ions shielding the negative charges through coordination with the sulfate half-ester groups. The colloidal stability was not deteriorated by functionalization with Ln^{3+} ions demonstrated by that the suspensions were stable when observed by the naked eye, and no precipitation was observed.

Steady shear viscosity evaluation (Fig. 6) revealed qualitative and quantitative differences between Na-CNC and the trivalent lanthanide cation CNC suspensions. An increase of up to three orders of magnitude

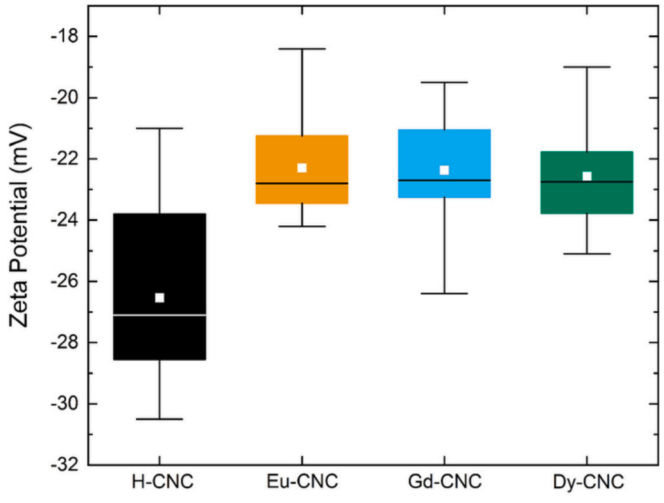

Fig. 5. Zeta potential of H-CNC and Ln-CNC suspensions. The line and square inside each box represent the median and the mean, respectively.

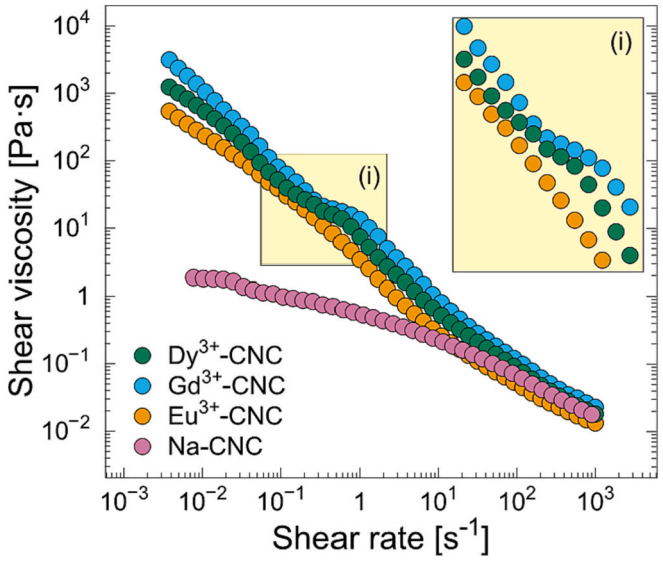

Fig. 6. Steady shear viscosity functions of CNC suspensions.

was measured for Eu-CNCs, Gd-CNCs, and Dy-CNC relative to Na-CNCs in the low shear range. The Na-CNC viscosity function exhibited a zero-shear Newtonian plateau, followed by a shear thinning characteristic of isotropic CNC suspensions. In contrast, Ln-CNC viscosity was described by three-region viscosity functions characteristic of liquid crystalline systems. Some structural formations were detected particularly in the case of Dy^{3+} and Gd^{3+} (see the detail in Fig. 6). For shear rates above 10 1 s^{-1}, the viscosity functions started to converge, most likely because substantial shear led to the breakdown of already formed networks and the constituents were oriented in the direction of flow. We performed steady shear tests using a cross-polarized optical setup,(Kádár et al., 2020) but no evidence of liquid crystalline structures, which would be apparent in the evolution of the polarization patterns, was found at flow scale.

Oscillatory shear measurements (Figs. 7 and 8) further confirmed the presence of a gel network in the Ln^{3+} CNC suspensions. Na-CNC displayed a predominantly viscous behavior ($G'' > G'$), while the lanthanide CNC suspensions were clearly above their respective gel points, with $G' > G''$ across the entire angular frequency range investigated. Furthermore, in the transition to the nonlinear region in strain sweep tests, a weak strain overshoot (WSO), which indicates a local increase in G', was recorded for the Ln-CNC suspensions, with Gd-CNCs and Dy-CNCs showing the most prominent WSO (see detail in Fig. 7). The presence of WSO is usually interpreted as a jamming microstructure prior to yielding.

3.4. Functionality of Ln-CNC systems

In the emission spectra recorded at 395 nm, the CNC film showed a wide absorbance band at 470 nm, which was present also in the Ln-CNCs (Fig. 9). Eu-CNCs revealed emission bands at 590, 613 and 697 nm, corresponding to the electric dipole transition of $^5D_0 \rightarrow {}^7F_J$ in Eu^{3+} ions. The peak at 613 nm corresponds to Eu^{3+} red luminescence emission. (Yang et al., 2018).

Gd^{3+} was anticipated to equip the cellulose host with a magnetic functionality. Analysis of Gd-CNC indicated an extremely shortened MRI T1 relaxation time (from 2580 +/− 50 ms to unidentifiable in this set-up and measurement) and a shortened T2 relaxation time (from 350 +/− 70 ms to 13.3 +/− 3 ms). The lanthanide modified CNCs appear to be effective contrast agents as evidenced by the reduction of T1/T2 relaxation times. For that, the concentration with respect to the relaxation time, viscosity, relaxivity rates, their ratio, and benchmarking to conventional lanthanide based contrast agents are required, however, outside of the scope of this study.

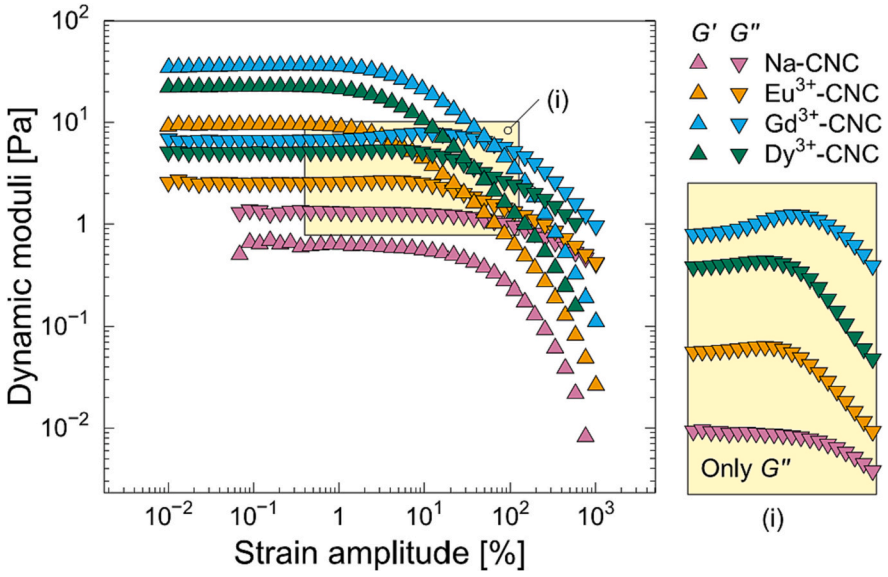

Fig. 7. Oscillatory shear strain amplitude sweep tests presenting the dynamic moduli against shear strain amplitude as a function of the counter cation tested.

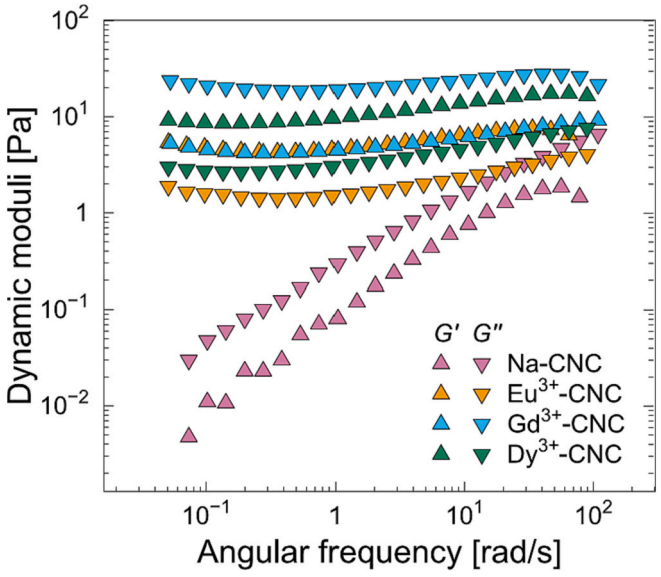

Fig. 8. Oscillatory shear linear viscoelastic frequency sweep tests presenting the dynamic moduli against angular frequency as a function of counter cation tested.

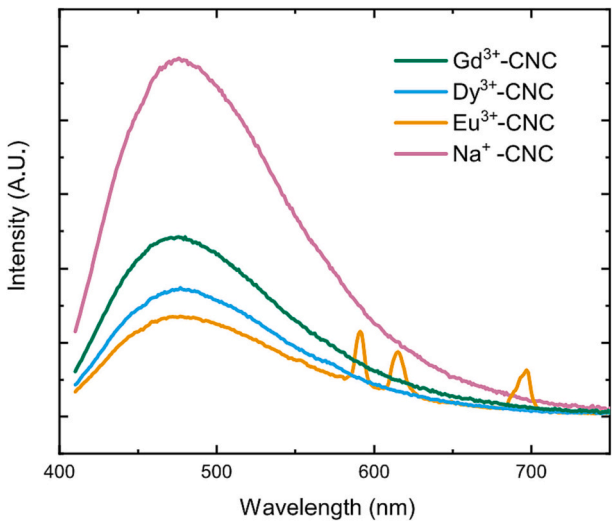

Fig. 9. Emission spectra of Ln-CNC films. Emission was recorded in room temperature for Na-CNCs (430 nm), Eu-CNCs (464 nm), Gd-CNCs (410 nm), and Dy-CNCs (410 nm) following 395 nm excitation.

4. Conclusions

We have demonstrated a facile cation exchange pathway for functionalization of cellulose with lanthanide cations and provided knowledge about their coordination to the sulfate groups on the CNC surface. While Eu^{3+} coordinated with all available sulfate groups, while Gd^{3+} showed 82 % and Dy^{3+} 41 % charge neutralization of the sulfate groups, i.e. not all of the protons have been exchanged by these ions. Eu^{3+} provided optical functionality with metal centered emission, while Gd^{3+} efficiently shortened the magnetic relaxation time. In contrast, Dy^{3+} did not lead to functionality. The selected lanthanides are relatively non-toxic with LD_{50} values in several thousands of mg/kg. However, for wide spread use, attention needs to be directed in sustainable mining and sourcing via recycling. The concept of using the simple cation exchange phenomenon to modify cellulose in various ways has potential to be expanded within the limits of functional groups and we contribute here with demonstrations of establishing this concept.

CRediT authorship contribution statement

Panagiotis Spiliopoulos: Conceptualization, Investigation, Methodology, Writing – original draft, Writing – review & editing. **Saül Llàcer Navarro:** Investigation, Writing – review & editing. **Eliott Orzan:** Investigation, Visualization, Writing – review & editing. **Reza Ghanbari:** Investigation, Writing – review & editing. **Rudolf Pietschnig:** Conceptualization, Investigation, Methodology, Writing – original draft, Writing – review & editing. **Clemens Stilianu:** Investigation, Writing – review & editing. **Stefan Spirk:** Investigation, Writing – review & editing. **Andreas Schaefer:** Investigation, Methodology, Writing – review & editing. **Roland Kádár:** Investigation, Methodology, Writing – original draft, Writing – review & editing. **Tiina Nypelö:** Conceptualization, Funding acquisition, Investigation, Methodology, Project administration, Resources, Supervision, Writing – original draft, Writing – review & editing.

Declaration of competing interest

The authors declare that they have no known competing financial interests or personal relationships that could have appeared to influence the work reported in this paper.

Data availability

Data will be made available on request.

Acknowledgements

We are grateful for funding from the Excellence Initiative Nano at the Chalmers University of Technology and Wallenberg Wood Science Center via Alice and Knut Wallenberg foundation and the Chalmers Foundation. The Chalmers Material Analysis Laboratory (CMAL) is acknowledged for providing access to the fluorescence microscope and scanning electron microscope. Katarina Logg is acknowledged for performing fluorescence microscopy measurements. We thank Carlos Benitez Martin, Chalmers University of Technology, for fluorometer measurements and analysis. We acknowledge Hermann Scharfetter for access to magnetic resonance measurements.

Appendix A. Supplementary data

Supplementary data to this article can be found online at https://doi.org/10.1016/j.carbpol.2024.121857.

References

Abitbol, T., Kloser, E., & Gray, D. G. (2013). Estimation of the surface sulfur content of cellulose nanocrystals prepared by sulfuric acid hydrolysis. *Cellulose, 20*(2), 785–794.

Beck, S., Méthot, M., & Bouchard, J. (2015). General procedure for determining cellulose nanocrystal sulfate half-ester content by conductometric titration. *Cellulose, 22*(1), 101–116.

Brauer, G. (1960). *Handbuch der präparativen anorganischen Chemie*. No Title.

Campbell, J., & Papp, T. (2001). Widths of the atomic K–N7 levels. Atomic Data and Nuclear Data Tables, 77(1), 1–56.

Cotton, S. (2013). *Lanthanide and actinide chemistry*. John Wiley & Sons.

Denisenko, Y. G., Sedykh, A. E., Oreshonkov, A. S., Molokeev, M. S., Azarapin, N. O., Sal'nikova, E. I., … Müller-Buschbaum, K. (2022). Europium (II) sulfate EuSO4: Synthesis methods, crystal and electronic structure, luminescence properties. *European Journal of Inorganic Chemistry, 2022*(12), Article e202200043.

Dong, X. M., & Gray, D. G. (1997). Effect of Counterions on ordered phase formation in suspensions of charged Rodlike cellulose crystallites. *Langmuir, 13*(8), 2404–2409.

Dong, X. M., Revol, J.-F., & Gray, D. G. (1998). Effect of microcrystallite preparation conditions on the formation of colloid crystals of cellulose. *Cellulose, 5*(1), 19–32.

Fan, W., Du, J., Kou, J., Zhang, Z., & Liu, F. (2018). Hierarchical porous cellulose/lanthanide hybrid materials as luminescent sensor. *Journal of Rare Earths, 36*(10), 1036–1043.

Habibi, Y., Lucia, L. A., & Rojas, O. J. (2010). Cellulose nanocrystals: Chemistry, self-assembly, and applications. *Chemical Reviews, 110*(6), 3479–3500.

Hummel, H. U., Fischer, E., Fischer, T., Joerg, P., & Pezzei, G. (1993). Structure and thermal behavior of gadolinium (III) sulfate Octahydrate Gd2 (SO4) 3× 8 H2O. *ChemInform, 24*(27), no–no.

Johansson, L. S., Campbell, J. M., & Rojas, O. J. (2020). Cellulose as the in situ reference for organic XPS. Why? Because it works. *Surface and Interface Analysis, 52*(12), 1134–1138.

Kádár, R., Fazilati, M., & Nypelö, T. (2020). Unexpected microphase transitions in flow towards nematic order of cellulose nanocrystals. *Cellulose, 27*(4), 2003–2014.

Klemm, D., Philipp, B., Heinze, T., Heinze, U., & Wagenknecht, W. (1998). *Comprehensive cellulose chemistry, Vol. 1: Fundamentals and analytical methods; Vol. 2: Functionalization of cellulose*.

Llàcer Navarro, S., Nakayama, K., Idström, A., Evenäs, L., Ström, A., & Nypelö, T. (2021). The effect of sulfate half-ester groups on cellulose nanocrystal periodate oxidation. *Cellulose, 28*, 9633–9644.

Llàcer Navarro, S., Tölgo, M., Olsson, L., & Nypelö, T. (2023). Carboxylation of sulfated cellulose nanocrystals by family AA9 lytic polysaccharide monooxygenases. *Cellulose, 30*, 1–17.

Mercier, F., Alliot, C., Bion, L., Thromat, N., & Toulhoat, P. (2006). XPS study of Eu (III) coordination compounds: Core levels binding energies in solid mixed-oxo-compounds EumXxOy. *Journal of Electron Spectroscopy and Related Phenomena, 150*(1), 21–26.

Miao, M., Zhao, J., Feng, X., Cao, Y., Cao, S., Zhao, Y., Ge, X., Sun, L., Shi, L., & Fang, J. (2015). Fast fabrication of transparent and multi-luminescent TEMPO-oxidized nanofibrillated cellulose nanopaper functionalized with lanthanide complexes. *Journal of Materials Chemistry C, 3*(11), 2511–2517.

Moulder, J., Stickle, W., Sobol, P., & Bomben, K. (1992). *Handbook of X-ray photoelectron spectroscopy: A reference book of standard spectra for identification and interpretation of XPS data*. Eden Prairie, Minnesota, USA: Perkin-Elmer Corporation, Physical Electronics Division.

Petschacher, P., Ghanbari, R., Sampl, C., Wiltsche, H., Kádár, R., Spirk, S., & Nypelö, T. (2022). Dynamic and static assembly of sulfated cellulose nanocrystals with alkali metal counter cations. *Nanomaterials, 12*(18), 3131.

Prathapan, R., Thapa, R., Garnier, G., & Tabor, R. F. (2016). Modulating the zeta potential of cellulose nanocrystals using salts and surfactants. *Colloids and Surfaces A: Physicochemical and Engineering Aspects, 509*, 11–18.

pubchem.org. Dysprosium chloride. https://pubchem.ncbi.nlm.nih.gov/compound/66207 Accessed.

pubchem.org. Europium chloride. https://pubchem.ncbi.nlm.nih.gov/compound/24809 Accessed.

pubchem.org. Gadolinium chloride. https://pubchem.ncbi.nlm.nih.gov/compound/61486 Accessed.

Rim, K. T., Koo, K. H., & Park, J. S. (2013). Toxicological evaluations of rare earths and their health impacts to workers: A literature review. *Safety and Health at Work, 4*(1), 12–26.

Roman, M., & Winter, W. T. (2004). Effect of sulfate groups from sulfuric acid hydrolysis on the thermal degradation behavior of bacterial cellulose. *Biomacromolecules, 5*(5), 1671–1677.

Sixta, H. (2006). *Handbook of pulp*. Wiley-vch.

Skwierczyńska, M., Runowski, M., Kulpiński, P., & Lis, S. (2019). Modification of cellulose fibers with inorganic luminescent nanoparticles based on lanthanide (III) ions. *Carbohydrate Polymers, 206*, 742–748.

Szczeszak, A., Skwierczyńska, M., Przybylska, D., Runowski, M., Śmiechowicz, E., Erdman, A., Ivashchenko, O., Grzyb, T., Lis, S., & Kulpiński, P. (2020). Upconversion luminescence in cellulose composites (fibres and paper) modified with lanthanide-doped SrF 2 nanoparticles. *Journal of Materials Chemistry C, 8*(34), 11922–11928.

Teo, R. D., Termini, J., & Gray, H. B. (2016). Lanthanides: Applications in cancer diagnosis and therapy: Miniperspective. *Journal of Medicinal Chemistry, 59*(13), 6012–6024.

Vanderfleet, O. M., Reid, M. S., Bras, J., Heux, L., Godoy-Vargas, J., Panga, M. K., & Cranston, E. D. (2019). Insight into thermal stability of cellulose nanocrystals from new hydrolysis methods with acid blends. *Cellulose, 26*, 507–528.

Wang, N., Ding, E. Y., & Cheng, R. S. (2007). Thermal degradation behaviors of spherical cellulose nanocrystals with sulfate groups. *Polymer, 48*(12), 3486–3493.

Wang, Q., Chen, G., Yu, Z., Ouyang, X., Tian, J., & Yu, M. (2018). Photoluminescent composites of lanthanide-based nanocrystal-functionalized cellulose fibers for anticounterfeiting applications. *ACS Sustainable Chemistry & Engineering, 6*(11), 13960–13967.

Werts, M. H. (2005). Making sense of lanthanide luminescence. *Science Progress, 88*(2), 101–131.

Xue, B., Zhang, Z., Sun, Y., Wang, J., Jiang, H., Du, M., Chi, C., & Li, X. (2018). Near-infrared emissive lanthanide hybridized nanofibrillated cellulose nanopaper as ultraviolet filter. *Carbohydrate Polymers, 186*, 176–183.

Yang, Q., Zhang, C., Shi, Z., Wang, J., Xiong, C., Saito, T., & Isogai, A. (2018). Luminescent and transparent nanocellulose films containing europium carboxylate groups as flexible dielectric materials. *ACS Applied Nano Materials, 1*(9), 4972–4979.

Ye, J., Wang, B., Xiong, J., & Sun, R. (2016). Enhanced fluorescence and structural characteristics of carboxymethyl cellulose/Eu (III) nano-complex: Influence of reaction time. *Carbohydrate Polymers, 135*, 57–63.

Zhang, S., Liu, G., Chang, H., Li, X., & Zhang, Z. (2019). Optical haze nanopaper enhanced ultraviolet harvesting for direct soft-fluorescent emission based on lanthanide complex assembly and oxidized cellulose nanofibrils. *ACS Sustainable Chemistry & Engineering, 7*(11), 9966–9975.

Zhong, L., Fu, S., Peng, X., Zhan, H., & Sun, R. (2012). Colloidal stability of negatively charged cellulose nanocrystalline in aqueous systems. *Carbohydrate Polymers, 90*(1), 644–649.